International Journal of Modern Physics C
Vol. 29, No. 5 (2018) 1840007 (11 pages)

DOI: 10.1142/S0129183118400077

World Scientific
www.worldscientific.com

Individual T1-weighted/T2-weighted ratio brain networks: Small-worldness, hubs and modular organization

Huijun Wu[*,‡,§,¶], Hao Wang[*,‖] and Linyuan Lü[*,†,**]

[*]*Institute of Fundamental and Frontier Sciences*
University of Electronic Science and Technology of China
Chengdu 611731, P. R. China

[†]*Alibaba Research Center for Complexity Sciences*
Hangzhou Normal University, Hangzhou 311121, P. R. China

[‡]*Center for Cognition and Brain Disorders*
Hangzhou Normal University
Hangzhou 311121, P. R. China

[§]*Zhejiang Key Laboratory for Research in*
Assessment of Cognitive Impairments
Hangzhou 311121, P. R. China
[¶]*huijun.psyc@gmail.com*
[‖]*h.wang.psyc@gmail.com*
[**]*linyuan.lv@gmail.com*

Received 30 September 2017
Accepted 14 March 2018
Published 30 May 2018

Applying network science to investigate the complex systems has become a hot topic. In neuroscience, understanding the architectures of complex brain networks was a vital issue. An enormous amount of evidence had supported the brain was cost/efficiency trade-off with small-worldness, hubness and modular organization through the functional MRI and structural MRI investigations. However, the T1-weighted/T2-weighted (T1w/T2w) ratio brain networks were mostly unexplored. Here, we utilized a KL divergence-based method to construct large-scale individual T1w/T2w ratio brain networks and investigated the underlying topological attributes of these networks. Our results supported that the T1w/T2w ratio brain networks were comprised of small-worldness, an exponentially truncated power–law degree distribution, frontal-parietal hubs and modular organization. Besides, there were significant positive correlations between the network metrics and fluid intelligence. Thus, the T1w/T2w ratio brain networks open a new avenue to understand the human brain and are a necessary supplement for future MRI studies.

Keywords: Brain network; small-worldness; hubs; modules; T1w/T2w ratio.

PACS Nos.: 64.60.aq, 84.35.+1, 87.19.1f.

[**]Corresponding author.

1. Introduction

In recent years, network approaches have become a research hotspot of physics, engineering, information, biological, and neuroscience.[1] Modern brain imaging techniques have significantly improved our understanding of the microstructural properties of the human brain. Notably, several lines of evidence had suggested that the brain function relied on integrative processes and dynamic interactions of many regions, rather than solely be attributable to the individual areas. Hence, the brain was particularly amenable to network analysis. At present, combining network approaches and brain imaging techniques has catalyzed a network neuroscience view on the human brain structure and function. The human networks could be constructed using different imaging techniques [e.g. functional MRI (fMRI), diffusion tensor imaging (DTI) and structural MRI (sMRI)]. fMRI is used to construct the functional brain networks by estimating statistical dependence between the signals measured in each region.[2] DTI and sMRI are also used to build the structural and morphological brain networks by fiber tracking (i.e. physical wiring)[3] and calculating the interregional morphological similarity,[4,5] respectively. Besides the fMRI, DTI and sMRI, the T1w/T2w ratio image which is a reasonable estimate of relative myelin content across the cortical surface (myelin maps),[6] has attracted the attention of the investigator. It should be noted that a previous study proved aerobic glycolysis and synaptic plasticity were associated with the T1w/T2w ratio,[7] and the T1w/T2w ratio reliably mapped brain structural differences between patients and healthy controls, which was found to identify more robust markers than the individual T1w or T2w images in schizophrenia.[8] However, the topological attributes of T1w/T2w ratio brain networks have been less explored so far. Here, we performed the same framework proposed by Kong and Wang[4,5] to construct the individual large-scale T1w/T2w ratio brain networks and investigated the small-worldness, hubs and modular organization of these networks. As far as we know, this is the first study to examine the individual T1w/T2w ratio images from a network perspective. And it will be a necessary complement for the comprehension of the human brain and provide a new avenue to explore the relationship between myelin-associated genes, human cognition, behavior, and the T1w/T2w ratio networks.

2. Data and Method

2.1. *Participants*

We downloaded the publicly available Washington University Minnesota (WU-Min) Human Connectome Project (HCP) data (Principal Investigators: David Van Essen and Kamil Ugurbil; 1U54MH091657) which was funded by the 16 NIH Institutes and Centers that support the NIH Blueprint for Neuroscience Research, and by the McDonnell Center for Systems Neuroscience at Washington University;[9] these DICOM files were converted to NIfTI format using the dcm2nii utility which was developed by Chris Rorden (http://www.nitrc.org/projects/mricron). We randomly

selected 95 participants from the S1200 release of the HCP. Informed consent was obtained from all the participants, and all analyses were approved by the Yale and Rutgers IRBs.

2.2. *MRI data acquisition*

The HCP collected the structural scans with the following parameters: T1-w (0.7-mm isotropic resolution, TR = 2400 ms, TE = 2.14 ms, flip angle = 8, in-plane field of view = 224 × 224, acquisition time = 7 min 40 s) and T2-w (0.7 mm isotropic resolution, TR = 3200 ms, TE = 565 ms, variable flip angle, in-plane field of view = 224 × 224, acquisition time = 8 min 24 s). The online reference manual provides complete details of all HCP acquisition (https://www.humanconnectome. org).

2.3. *T1w/T2w ratio calculation*

T1w and T2w images were preprocessed and combined using a dedicated workflow.[8,10] The workflow included bias correction and intensity calibration on each of the two images and the subsequent calculation of the ratio between preprocessed T1w and T2w images. Finally, we spatially normalized T1w/T2w images to the Montreal Neurological Institute space. The entire processing of the T1w/T2w image was conducted using the MRTool (https://www.nitrc.org/projects/mrtool, version 1.4.2) implemented in the SPM12 (version r7219) software (http://www.fil.ion.ucl.ac.uk/spm/software/spm12, Wellcome Trust Centre for Neuroimaging, London, UK).

2.4. *Construction and analysis of individual T1w/T2w ratio brain networks*

We utilized the T1w/T2w ratio images to construct large-scale brain networks. The two fundamental steps to build human brain network was to define the nodes and edges. Here, we utilized widely used structural brain templates [i.e. Anatomical Automatic Labeling (AAL-90) atlas][11] as the nodes and the similarity of each pair nodes' T1w/T2w ratio as the edges.[12] In detail, first, we divided the brain into 90 regions of interest (ROIs) and estimated the probability density function for each ROI.[13] Second, through the integral transformations over the sample point space of probability density function, we obtained the probability distribution function (PDF). Third, we performed a symmetric KL divergence (statistical similarity) between the PDFs of each pair of ROIs[5,12] to define the edges. Thus, the T1w/T2w ratio connectivity matrices were generated for each participant,[5] see flow chart (Fig. 1). Because the binary network is easy to characterize and to construct appropriate null networks for benchmarking,[14] in current study, we only focused on the binary networks and binarized the T1w/T2w ratio connectivity matrix using a sparsity threshold value 20% (i.e. only keep the top 20% edges in the network) for each participant. Subsequently, for each network, a series of global (clustering coefficient, C; characteristic path length, L; and modularity, Q) and nodal (degree,

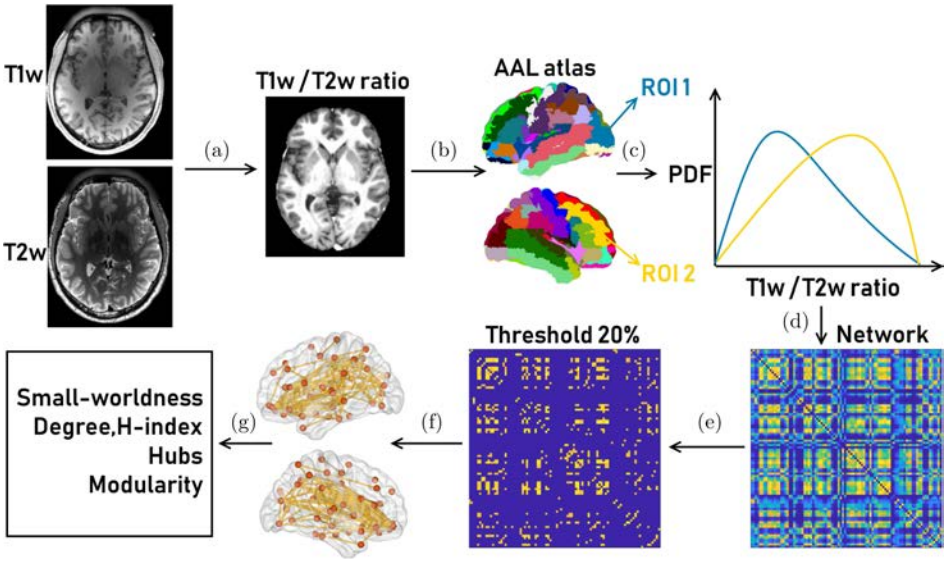

Fig. 1. (Color online) The workflow of the analytical process in the current study. In short, we first calculated the T1w/T2w ratio for each participant (a). Utilizing the AAL-90 atlas to parcellate the T1w/T2w ratio images (b). For each brain region, we estimated its probability distribution function (c). Further, we used a KL divergence-based method to construct large-scale individual T1w/T2w ratio brain networks (d). After thresholding the network at sparsity value 20% (e), the visualization of the binary network was presented (f). Finally, we calculated a serial network index to explore the small-worldness, hubness, and module of the T1w/T2w ratio brain network (g).

H-index, coreness) metrics[15] were calculated with the BCT toolbox[14] and our home-made code.

The cluster coefficient of a node is defined as

$$C_i = \frac{2e_i}{k_i(k_i - 1)}, \tag{1}$$

where e_i is the number of links within its neighborhoods, k_i is its degree. The global cluster coefficient is the mean value of the nodes' cluster coefficient.

The characteristic path length of the network is

$$L = \frac{1}{N} \sum_{i \in N} L_i, \tag{2}$$

where L_i is the average distance between node i and all other nodes.

The Modularity of the network can be denoted as

$$Q = \sum_{u \in M} \left[e_{\mathrm{uu}} - \left(\sum_{v \in M} e_{\mathrm{uv}} \right)^2 \right], \tag{3}$$

where M is the number of the modules, e_{uu} is the fraction of edges in the network that connect nodes in the same module, and e_{uv} is the fraction of all edges in the network that link nodes in the different modules.

The H-index of a node is defined as the maximum value h such that there exists at least h neighbors, each with degree $\geq h$. where $k_{j_1}, k_{j_2}, k_{j_3}, \ldots, k_{j_{k_i}}$ is the sequence of degree values of v_i's neighbors. The zero-order H-index is equal to its degree and Lü *et al.*[15] proved that the H-index of every node will converge to its coreness after finite steps.

$$h_i = H(k_{j_1}, k_{j_2}, k_{j_3}, \ldots, k_{j_{k_i}}) \tag{4}$$

Detailed explanations and formulas of these metrics could be seen from the methodological review[14] and Lü *et al.*'s work.[15]

3. Results and Discussion

3.1. *Small-worldness*

Small-worldness has been widely applied to the analysis of neuroimaging and other complex network data as part of the rapid growth of the new field of connectomics. To determine whether the T1w/T2w ratio brain networks were small-worldness,[16] we compared the clustering coefficient, C, and characteristic path length, L with the average values from 100 corresponding randomized networks with preserved degree distribution.[17,18] Thus, we generated $\gamma = C/Cr$, $\lambda = L/Lr$, and $\sigma = \gamma/\lambda$. If $\gamma > 1$, $\lambda \approx 1$ and $\sigma > 1$ were simultaneously met, the network owned the small-worldness. Compared with 100 random networks for each participant, the T1w/T2w ratio brain networks exhibited mean value and standard deviation for γ (1.662 ± 0.460), λ (1.297 ± 0.074), and σ (1.288 ± 0.374). Notably, there were 20 participants with a $\sigma < 1$ (see Fig. 2). Besides, we also calculated the small-world propensity which could be regarded as a revised version of small-worldness.[19] Networks would be considered as small-worldness if they have small-world propensity $0.4 < \Phi < 1$. Here, the results showed that the mean and standard deviation for Φ is 0.526 ± 0.209. Taken together, these findings implied small-worldness was retained for the T1w/T2w ratio brain networks.

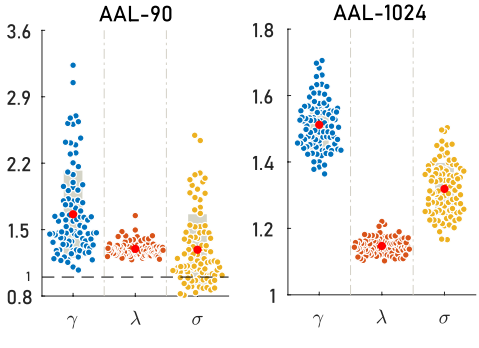

Fig. 2. (Color online) The small-worldness of the network. The mean value and standard deviation is $\gamma(1.662 \pm 0.460)$, $\lambda(1.297 \pm 0.074)$, and $\sigma(1.288 \pm 0.374)$ for AAL-90 atlas, and is γ (1.512 ± 0.074), λ (1.147 ± 0.024), and σ (1.319 ± 0.078) for AAL-1024 atlas.

3.2. *Degree distribution and Hubs*

The degree distribution is an important marker for the network development and resilience. Our results indicated the T1w/T2w ratio brain networks had an exponentially truncated power–law degree distribution (see Fig. 3), implying the probability of hubs (highly connected nodes) will be smaller than in a scale-free network but higher than in a random graph. Hubs played an essential role in massive communication, transshipment, switching within the system.[20] To detect the hubs' location in the T1w/T2w ratio brain networks, we calculated the nodal degree, H-index, and coreness centrality. For each metric, we retained nodes which were at least one standard deviation higher than the average nodal parameter of the network, and the common nodes across the three conditions were identified as potential hubs. The results showed that 17 hub nodes were identified, these nodes are mainly located in the frontal (9 nodes), parietal (4 nodes), occipital (2 nodes) and temporal (2 nodes) lobe. They were bilateral superior frontal gyrus, orbital part; middle frontal gyrus, orbital part; inferior frontal gyrus, triangular part (IFGtriang); median cingulate and para cingulate gyri (DCG); hippocampus (HIP); middle occipital gyrus; supramarginal gyrus (SMG); angular gyrus, and left superior frontal gyrus, medial orbital (see Fig. 4). These regions were comparable with the potential hubs reported in the previous morphological, structural and functional brain networks, for example, the IFGtriang, DCG, HIP, SMG, etc. were jointly identified.[1,5,21–24] Given that the brain hubs are easily attacked for a series of dysfunctions and disorders,[25,26] using the T1w/T2w ratio brain networks to investigate the altered hubs across some brain disorders may be an interesting project.

3.3. *Modularity*

Modularity (Q) is a measure of network segregation, by which nodes are subdivided into communities, or modules, to maximize intra-community edge strength in

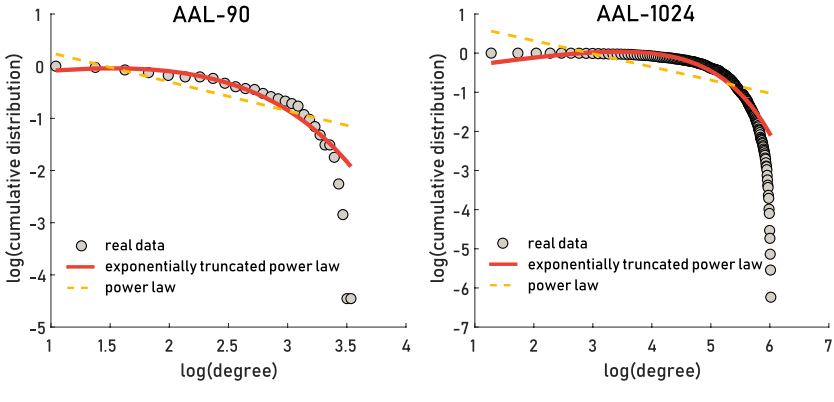

Fig. 3. (Color online) The degree distributions of networks (the log-log plot of the cumulative probability degree versus the degree). The results showed the T1w/T2w ratio brain networks had an exponentially truncated power-law degree distribution under both AAL-90 and AAL-1024 atlas.

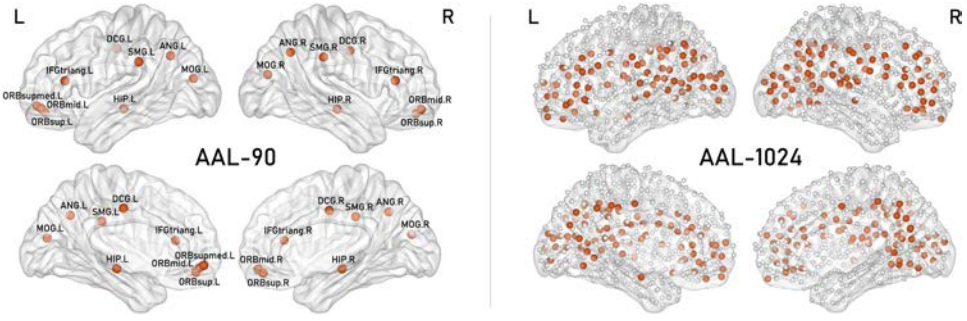

Fig. 4. (Color online) The hubs in the network. Seventeen hub nodes were identified, these nodes are mainly located in the frontal (9 nodes), parietal (4 nodes), occipital (2 nodes) and temporal (2 nodes) lobe for AAL-90 atlas. For AAL-1024 atlas, 158 hub nodes were identified, these nodes are mainly located in the default mode network. L, left hemisphere; R, right hemisphere. Figures were visualized with the BrainNet Viewer.[33]

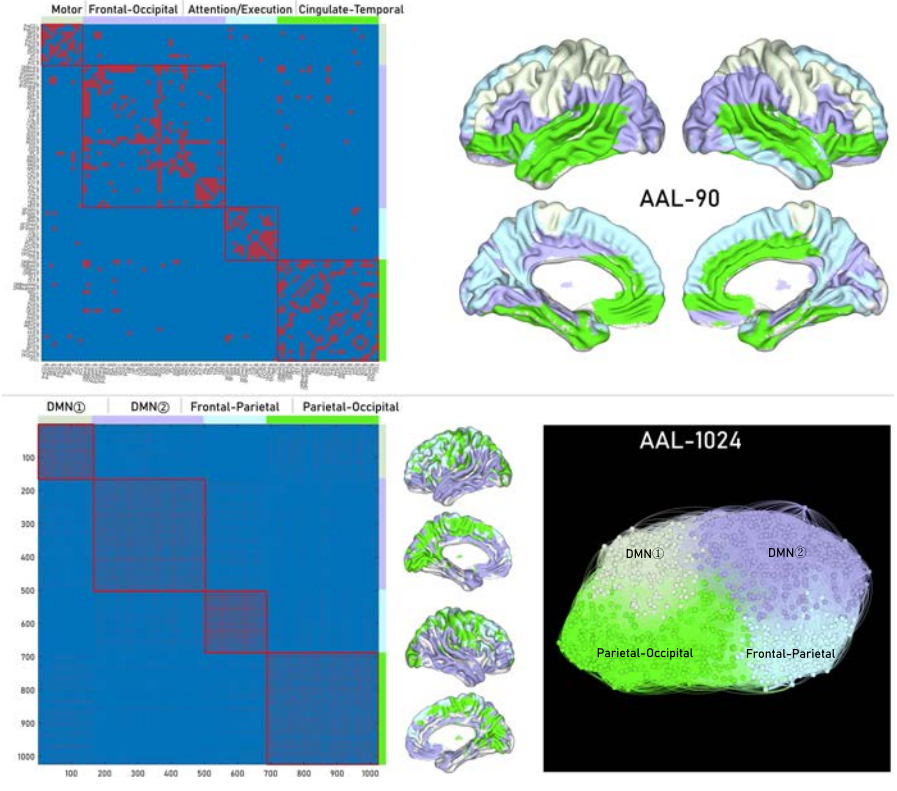

Fig. 5. (Color online) The modular organization of the network. For the AAL-90 atlas, four modules (Motor, Frontal-Occipital, Attention/Execution, Cingulate-Temporal) were obtained ($Q = 0.778$, Z-score = 59.030). For the AAL-1024 atlas, four modules (DMN① , DMN② , Frontal-Parietal, Parietal-Occipital) were found with a higher modularity ($Q = 0.817$, Z-score = 477.198). L, left hemisphere; R, right hemisphere.

comparison to a random network null model. To detect a stable consensus community structure, we first calculated the group average T1w/T2w ratio connectivity matrices and extracted the backbone matrix of the network.[27] Then we performed the Louvain algorithm 1000 times on the backbone matrix. A consensus matrix was created defining each element as the number of times that each node had been classified to the same module. Finally, we applied community algorithm on the consensus matrix and acquired a stable modular structure for the original network. Four modules (Motor, Frontal-Occipital, Attention/Execution, Cingulate-Temporal) were obtained ($Q = 0.778$, Z-score $= 59.030$) (see Fig. 5), which were similar with the modules derived from functional and diffusion MRI data, such as the Motor module, Frontal-Occipital module and Attention/Execution module.[23,28–30]

3.4. *Correlation between network metrics and fluid intelligence*

The previous study reported the significant correlation between the global efficiency of functional brain networks and intellectual performance.[31] Here, to provide more insights into the understanding and potential biological significance of the T1w/T2w ratio networks, we performed an exploration analysis and calculated the Pearson correlation between the network metrics (cluster coefficient, characteristic path length, mean nodal H-index, and mean nodal coreness) and the Penn Progressive Matrices: Number of Correct Responses (PMAT24_A_CR, fluid intelligence performance). The results showed there were significant positive correlations between the

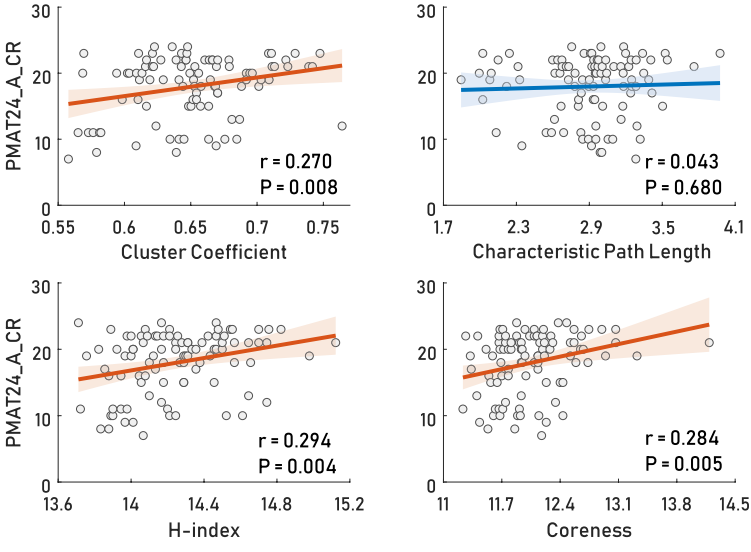

Fig. 6. (Color online) Correlation between network organization and fluid intelligence under the AAL-90 atlas. The results showed that there are significant positive correlations between the network metrics [cluster coefficient ($r = 0.270$, $P = 0.008$), H-index ($r = 0.294$, $P = 0.004$), and coreness ($r = 0.284$, $P = 0.005$)] and the fluid intelligence performance.

network metrics [cluster coefficient ($r = 0.270$, $P = 0.008$), H-index ($r = 0.294$, $P = 0.004$), and coreness ($r = 0.284$, $P = 0.005$)] and the fluid intelligence performance (see Fig. 6).

4. Validating the Reproducibility

4.1. *Effect of different parcellation schemes*

It should be noted that the fundamental first step towards constructing brain networks is how to define network nodes and to select the appropriate measures to express their connectivity. The definition of node is sensitivity to the subsequent network analyses, and different parcellation strategies can result in different network measures for the same imaging data set.[32] There were many parcellation strategies, including atlas-based, random partitions, voxel-based, and clustering approaches. Here, we parcellated the AAL atlas into 1024 random anatomical ROI, with approximately the same number of voxels in each ROI, to estimate the robustness of our results against different parcellation schemes. The results showed the T1w/T2w ratio brain networks also owned the small-worldness, hubs, and modular organization. In detail, for the small-worldness, the mean and standard deviation for γ is (1.512 ± 0.074), $\lambda(1.147 \pm 0.024)$, and $\sigma(1.319 \pm 0.078)$, and the results indicated that the networks under the AAL-90 atlas exhibited significant higher $\gamma(t = 3.125, P = 0.002)$ and $\lambda(t = 19.778, P < 10^{-3})$ compared with the networks under the high resolution AAL$-$1024 atlas. However, there was no significant difference in $\sigma(t = -0.762, P = 0.448)$ between the AAL$-$90 and AAL$-$1024 atlas. For the small-world propensity, the results showed the mean and standard deviation is 0.677 ± 0.091. The hubs mainly located in default model network and four modules (DMN ① , DMN ② , Frontal-Parietal, Parietal-Occipital) were found with a higher modularity ($Q = 0.817$, Z$-$score $= 477.198$), and we did not find the significant correlation between any network metrics with the fluid intelligence (see Figs. 2–5).

4.2. *Effect of different sparsity threshold*

Before calculating the topological characterization of the derived T1w/T2w ratio connectivity matrices, we discarded link weights using a thresholding procedure to derive the binary networks. Because different threshold values could produce different results, we also reproduced the results using different sparsity values at 10% and 30%. For the small-worldness at 10% sparsity level, the mean and standard deviation for γ is (1.986 ± 0.726), λ (1.637 ± 0.162), and σ (1.225 ± 0.463). Notably, there were 29 participants with a $\sigma < 1$, which indicated no small-worldness at the 10% sparsity. For the small-worldness at 30% sparsity level, the mean and standard deviation is $\gamma(1.503 \pm 0.309)$, $\lambda(1.151 \pm 0.036)$, and $\sigma(1.309 \pm 0.276)$, and there were 9 participants showing the small-worldness $\sigma < 1$. Then, 17 hubs and 19 hubs were identified for sparsity at 10% and 30%, separately. To our surprise, the intersection of the identified hubs was as well as the hubs reported at 20% sparsity level. Besides,

our results showed a positive correlation between the network coreness and the fluid intelligence at 10% sparsity level.

5. Conclusion

We focused on the ratio of T1w/T2w image which was a valid proxy for myelin content. As far as we know, the current work provided the first evidence of small-worldness, exponentially truncated power–law degree distribution, frontal-parietal hubs and modular organization in large-scale brain networks employing T1w/T2w ratio images from MRI. The results were compatible with the previous brain network studies using other modal brain images, thus opening a new avenue toward understanding the human T1w/T2w ratio image and will aid the interpretation of future brain network studies. The future project can inspect whether the T1w/T2w ratio networks significantly change during some inflammatory–related diseases and aging and whether the T1w/T2w ratio networks significantly correlate with the participant's cognition, behavior, and genes.

Acknowledgments

This work is supported by the National Natural Science Foundation of China (Nos. 11622538, 61673150), and the Zhejiang Provincial Natural Science Foundation of China (No. LR16A050001).

References

1. S. Achard, R. Salvador, B. Whitcher, J. Suckling and E. Bullmore, *J. Neurosci.* **26**, 63 (2006).
2. B. Biswal, F. Z. Yetkin, V. M. Haughton and J. S. Hyde, *Magn. Reson. Med.* **34**, 537 (1995).
3. P. Hagmann, M. Kurant, X. Gigandet, P. Thiran, V. J. Wedeen, R. Meuli and J. P. Thiran, *PLoS One* **2**, e597 (2007).
4. X. Z. Kong, Z. Liu, L. Huang, X. Wang, Z. Yang, G. Zhou, Z. Zhen and J. Liu, *PLoS One* **10**, e0141840 (2015).
5. H. Wang, X. Jin, Y. Zhang and J. Wang, *Brain Behav.* **6**, e00448 (2016).
6. M. F. Glasser and D. C. Van Essen, *J. Neurosci.* **31**, 11597 (2011).
7. M. F. Glasser, M. S. Goyal, T. M. Preuss, M. E. Raichle and D. C. Van Essen, *Neuroimage* **93**, 165 (2014).
8. M. Ganzetti, N. Wenderoth and D. Mantini, *Neuroradiology* **57**, 917 (2015).
9. D. C. Van Essen, S. M. Smith, D. M. Barch, T. E. Behrens, E. Yacoub, K. Ugurbil and W.-M. H. Consortium, *Neuroimage* **80**, 62 (2013).
10. M. Ganzetti, N. Wenderoth and D. Mantini, *Front. Hum. Neurosci.* **8**, 671 (2014).
11. N. Tzourio-Mazoyer, B. Landeau, D. Papathanassiou, F. Crivello, O. Etard, N. Delcroix, B. Mazoyer and M. Joliot, *Neuroimage* **15**, 273 (2002).
12. X. Z. Kong, X. Wang, L. Huang, Y. Pu, Z. Yang, X. Dang, Z. Zhen and J. Liu, *J. Neurosci. Methods.* **237**, 103 (2014).
13. Z. I. Botev *et al.*, *Ann Stat.* **38**, 2916 (2010).
14. M. Rubinov and O. Sporns, *Neuroimage* **52**, 1059 (2010).

15. L. Lü, T. Zhou, Q. M. Zhang and H. E. Stanley, *Nat. Commun.* **7**, 10168 (2016).
16. D. J. Watts and S. H. Strogatz, *Nature* **393**, 440 (1998).
17. S. Maslov and K. Sneppen, *Science* **296**, 910 (2002).
18. R. Milo, S. Shen-Orr, S. Itzkovitz, N. Kashtan, D. Chklovskii and U. Alon, *Science* **298**, 824 (2002).
19. S. F. Muldoon, E. W. Bridgeford and D. S. Bassett, *Sci. Rep.* **6**, 22057 (2016).
20. L. Lü, D. Chen, X.-L. Ren, Q.-M. Zhang, Y.-C. Zhang and T. Zhou, *Phys. Rep.* **650**, 1 (2016).
21. R. L. Buckner, J. Sepulcre, T. Talukdar, F. M. Krienen, H. Liu, T. Hedden, J. R. Andrews-Hanna, R. A. Sperling and K. A. Johnson, *J. Neurosci.* **29**, 1860 (2009).
22. Y. He, Z. J. Chen and A. C. Evans, *Cereb. Cortex.* **17**, 2407 (2007).
23. P. Hagmann, L. Cammoun, X. Gigandet, R. Meuli, C. J. Honey, V. J. Wedeen and O. Sporns, *PLoS Biol* **6**, e159 (2008).
24. R. GeethaRamani and K. Sivaselvi, Human brain hubs (provincial and connector) identification using centrality measures, in *2014 Int. Conf. Recent Trends in Information Technology (ICRTIT)* (IEEE, Chennai, India, 10–12 April 2014), pp. 1–6
25. N. A. Crossley, A. Mechelli, J. Scott, F. Carletti, P. T. Fox, P. McGuire and E. T. Bullmore, *Brain* **137**, 2382 (2014).
26. C. J. Stam, *Nat. Rev. Neurosci.* **15**, 683 (2014).
27. N. J. Foti, J. M. Hughes and D. N. Rockmore, *PLoS One* **6**, e16431 (2011).
28. Z. J. Chen, Y. He, P. Rosa-Neto, J. Germann and A. C. Evans, *Cereb. Cortex.* **18**, 2374 (2008).
29. D. Meunier, S. Achard, A. Morcom and E. Bullmore, *Neuroimage* **44**, 715 (2009).
30. Y. He, J. Wang, L. Wang, Z. J. Chen, C. Yan, H. Yang, H. Tang, C. Zhu, Q. Gong, Y. Zang and A. C. Evans, *PLoS One* **4**, e5226 (2009).
31. M. P. van den Heuvel, C. J. Stam, R. S. Kahn and H. E. H. Pol, *J. Neurosci.* **29**, 7619 (2009).
32. A. Zalesky, A. Fornito, I. H. Harding, L. Cocchi, M. Yucel, C. Pantelis and E. T. Bullmore, *Neuroimage* **50**, 970 (2010).
33. M. Xia, J. Wang and Y. He, *PLoS One* **8**, e68910 (2013).